

RESEARCH ARTICLE

10.1029/2018MS001327

Key Points:

- Increase in atmospheric and oceanic resolution has largely independent effects on the simulated AMOC
- Increasing atmospheric resolution from T63 (~1.9°) to T127 (~0.9°) weakens the AMOC strength
- Changes in AMOC due to the ocean resolution relate to topography or model dynamics and have small effect on interhemispheric net transport

Correspondence to:

D. V. Sein, dmitry.sein@awi.de

Citation:

Sein, D. V., Koldunov, N. V., Danilov, S., Sidorenko, D., Wekerle, C., Cabos, W., et al. (2018). The relative influence of atmospheric and oceanic model resolution on the circulation of the North Atlantic Ocean in a coupled climate model. *Journal of Advances in Modeling Earth Systems*, 10. <https://doi.org/10.1029/2018MS001327>

Received 20 MAR 2018

Accepted 6 AUG 2018

Accepted article online 20 AUG 2018

The Relative Influence of Atmospheric and Oceanic Model Resolution on the Circulation of the North Atlantic Ocean in a Coupled Climate Model

Dmitry V. Sein^{1,2}, Nikolay V. Koldunov^{1,3}, Sergey Danilov^{1,4,5}, Dmitry Sidorenko¹, Claudia Wekerle¹, William Cabos⁶, Thomas Rackow¹, Patrick Scholz¹, Tido Semmler¹, Qiang Wang¹, and Thomas Jung^{1,7}

¹Alfred Wegener Institute, Helmholtz Centre for Polar and Marine Research, Bremerhaven, Germany, ²P. P. Shirshov Institute of Oceanology RAS, Moscow, Russia, ³MARUM—Center for Marine Environmental Sciences, Bremen, Germany, ⁴Department of Mathematics and Logistics, Jacobs University, Bremen, Germany, ⁵A. M. Obukhov Institute of Atmospheric Physics RAS, Moscow, Russia, ⁶Department of Physics and Mathematics, University of Alcala, Alcala, Spain, ⁷Institute of Environmental Physics, University of Bremen, Bremen, Germany

Abstract It is often unclear how to optimally choose horizontal resolution for the oceanic and atmospheric components of coupled climate models, which has implications for their ability to make best use of available computational resources. Here we investigate the effect of using different combinations of horizontal resolutions in atmosphere and ocean on the simulated climate in a global coupled climate model (Alfred Wegener Institute Climate Model [AWI-CM]). Particular attention is given to the Atlantic Meridional Overturning Circulation (AMOC). Four experiments with different combinations of relatively high and low resolutions in the ocean and atmosphere are conducted. We show that increases in atmospheric and oceanic resolution have clear impacts on the simulated AMOC, which are largely independent. Increased atmospheric resolution leads to a weaker AMOC. It also improves the simulated Gulf Stream separation; however, this is only the case if the ocean is locally eddy resolving and reacts to the improved atmosphere. We argue that our results can be explained by reduced mean winds caused by higher cyclone activity. Increased resolution of the ocean affects the AMOC in several ways, thereby locally increasing or reducing the AMOC. The finer topography (and reduced dissipation) in the vicinity of the Caribbean basin tends to locally increase the AMOC. However, there is a reduction in the AMOC around 45°N, which relates to the reduced mixed layer depth in the Labrador Sea in simulations with refined ocean and changes in the North Atlantic current pathway. Furthermore, the eddy-induced changes in the Southern Ocean increase the strength of the deep cell.

1. Introduction

As the availability of computational resources increases, coupled model simulations begin to employ increasingly high resolutions (HRs) in both their atmospheric and oceanic components. However, the question of how to best distribute resources between these two components of the climate system and thus make best use of the available computing resources remains largely unanswered. This question becomes even more difficult to answer if simulations use biogeochemical modules in ocean models or atmospheric chemistry modules in atmospheric models, which considerably slows down their throughput. In order to select optimal configurations, which adequately represent the dynamics required to answer specific scientific questions, it is imperative to know what we gain and lose with changes of the spatial resolution in different compartments of the Earth system.

The question of how the model resolution influences the performance of atmosphere-only, ocean-only, and climate models has been the subject of numerous recent studies. Increasing ocean model resolution in ocean models has a critical impact on the role that eddies play in the ocean heat budget and in the dynamics of major frontal systems (see, e.g., Iovino et al., 2016; Von Storch et al., 2016). Enhanced resolution improves the representation of narrow boundary currents (e.g., Marzocchi et al., 2015; Sein et al., 2017; Wang et al., 2018) and the connectivity between ocean basins (e.g., Chang et al., 2009). Increases of resolution in atmosphere-only models have also beneficial impacts on many aspects of the large-scale circulation and lead to a more realistic simulation of regional climate and small-scale phenomena (Jung et al., 2012, and Haarsma et al., 2016, for a comprehensive review).

©2018. The Authors.

This is an open access article under the terms of the Creative Commons Attribution-NonCommercial-NoDerivs License, which permits use and distribution in any medium, provided the original work is properly cited, the use is non-commercial and no modifications or adaptations are made.

For coupled climate models, a review by Hewitt et al. (2017) summarizes the present understanding of the mechanisms whereby the model resolution, especially in the ocean, may modify the simulated climate. In particular, they mention that many studies show a clear effect of the mesoscale ocean features in western boundary currents on the large-scale atmospheric state, while in other areas the possible effects from the mesoscale eddies on the large-scale atmospheric circulation remain unclear.

In a coupled system, effects from increased resolution vary depending on the driving mechanisms, time scales, and locations. For example, over most of the ocean the atmosphere is the main driver of changes in the sea surface temperature (SST); for frontal areas associated with western boundary currents, however, the opposite is true—the ocean drives the atmosphere (Bryan et al., 2010; Roberts et al., 2016) and effects from ocean mesoscale eddies are clearly imprinted on atmospheric fields (e.g., Ma et al., 2015, 2016).

There is emerging evidence from reanalysis and atmospheric simulations with prescribed HR SST that oceanic mesoscale features do modulate the atmospheric boundary layer (Frenger et al., 2013; Small et al., 2008), especially over ocean fronts. In lower latitudes, resolution in the ocean component of climate models has to be at least $1/4^\circ$ in order to start simulating some mesoscale turbulent activity including eddies, which can affect air-sea fluxes. According to Roberts et al. (2016), further increasing ocean resolution from $1/4^\circ$ to eddy resolving ($1/12^\circ$) does not change the air-sea flux relationship at small scales; yet it does have an impact on the mean ocean state. As found by Griffies et al. (2015), stronger vertical eddy heat transport in eddy resolving simulations essentially reduces the temperature drift, providing an argument for seamless representation of the ocean mesoscale dynamics. In turn, resolution in the atmospheric component also determines the atmospheric response to shifts in the ocean fronts (Smirnov et al., 2015). Higher atmospheric resolution leads to more intense vertical velocities over the ocean frontal areas, but only when it is sufficiently high to react to ocean eddies and fronts. Jung et al. (2006, 2012) found that cyclogenesis simulated by atmospheric models depends strongly on horizontal resolution for resolutions above 80 km, with higher resolutions showing reduced sensitivity. This means that the effect of resolution depends on the resolution itself and may differ depending on the range of resolutions studied.

Many changes associated with increased ocean resolution in coupled simulations result from a better representation of the North Atlantic Ocean. Indeed, storm tracks influencing climate over Europe have their origin in this area and their representation is affected by the simulated Gulf Stream position and hence ocean surface temperature. The strength of the Atlantic Meridional Overturning Circulation (AMOC), which is critical for determining the large-scale climate response to future climate forcing (He et al., 2017), depends on the model resolution in the North Atlantic (NA) too (Hewitt et al., 2016; Winton et al., 2014). While the AMOC is viewed as one of the main indicators in discussions of ocean response to changing climate, its modification due to refined resolution remains unclear. Hewitt et al. (2016) found that simultaneously increasing resolution in the ocean and atmosphere affects the strength of the poleward ocean heat transport and increases the AMOC. In experiments of Small et al. (2014), however, a simultaneous increase of resolution does not change considerably the mean state of the AMOC, while affecting interannual variability. On the other hand, Winton et al. (2014) find that increasing the ocean resolution while keeping the same atmospheric resolution leads to a decrease in the strength of the AMOC. Both studies refer to the representation of ocean topography in overflow region as a possible reason for changes in the AMOC. Given that AMOC has a strong contribution to climate variability and change, the question of how the AMOC responds to resolution is an important topic that merits systematic evaluation (e.g., Hewitt et al., 2017). Response of the AMOC to resolution change can depend on the range of the resolutions studied, and the answer obtained for the transition from $1/4^\circ$ to $1/12^\circ$ resolution does not necessarily hold for transition from 1° to $1/4^\circ$, which is mostly affordable for long-term climate simulations. Further complications may result from the fact that there are substantial changes in the model components in this range.

In this paper we investigate the sensitivity of the NA in general and the AMOC in particular to ocean and atmospheric resolutions using historical simulations performed with the Alfred Wegener Institute Climate Model (AWI-CM) following the HighResMIP protocol (Haarsma et al., 2016). The experimental setups allow us to separate effects from increased resolution in ocean versus atmosphere. We use spectral resolutions of T63/L95 (1.9° , 95 vertical layers) to T127/L95 ($\sim 0.9^\circ$, 95 vertical layers) for the atmosphere while the ocean component is configured with resolutions ranging from a nominal 1° to “equivalent” $1/4^\circ$. On the fine ocean mesh, however, the ocean resolution is finer than on traditional $1/4^\circ$ meshes at locations with high eddy

variability, at the expense of being coarser in the tropics and in wide areas of the subtropics where eddy variability is relatively weak (see the model setup section).

While the $1/4^\circ$ resolution in the ocean is still not fine enough to represent upward heat transport by mesoscale eddies that is responsible for many deep water biases in the ocean (Griffies et al., 2015), it is on the upper limit of what is presently affordable for most of the modeling groups contributing to the phase 6 of the Coupled Model Intercomparison Project (CMIP6). The use of unstructured meshes in the ocean component of AWI-CM allows one to concentrate the grid points in specific areas in order to obtain a locally eddy-resolving setup where it is needed without changing the total amount of grid points.

The next section describes the model setups and is followed by presenting results in section 3 and by discussion.

2. Model Setups

Model simulations presented below were performed with the AWI-CM. The sea ice-ocean component of the AWI-CM is the Finite Element Sea Ice-Ocean Model (FESOM1.4; Wang, Danilov, et al., 2014). FESOM is formulated on unstructured meshes allowing for spatially variable resolution. In previous studies (see Rackow et al., 2016; Sidorenko et al., 2015) it has been shown that the present-day mean climate and its variability simulated with AWI-CM are comparable to that of other models participated in CMIP5.

We use two ocean configurations of FESOM that differ only in the horizontal resolution (same as in Sein et al., 2016). The low-resolution (LR) configuration is based on a coarse mesh with a global nominal resolution of 1° , which is increased to about 25 km north of 50°N and to about $1/3^\circ$ in the equatorial belt, and is also moderately refined along the coasts (Figure 1a). This configuration of FESOM was used in the CORE-II intercomparison project, so the ocean model behavior is well documented (see, e.g., Danabasoglu et al., 2016; Wang et al., 2016a, 2016b; and other papers in the same CORE-II virtual special issue).

The HR configuration has a locally eddy-resolving mesh with the horizontal resolution varying according to the observed sea surface height (SSH) variability. The coarsest resolution is ~ 60 km, and the finest is ~ 10 km (see Figure 1b). In particular, the HR is set along the pathways of the main currents, including the Gulf Stream. While the number of nodes (1.3×10^6) is equivalent to a $1/4^\circ$ rectangular Mercator mesh (1.5×10^6 in total with only 1.0×10^6 wet), through focusing grid points in areas of interest, the resolution in these areas is as high as in traditional $1/10^\circ$ Mercator meshes. The areas where the HR setup is eddy permitting (resolution is in range 0.5–1.0 Rossby radius) or eddy resolving (resolution is less than a half of the Rossby radius) are shown in Figure 1c. More information about the mesh design of the HR configuration and its comparison to LR can be found in Sein et al. (2016).

Both ocean configurations have 47 unevenly spaced vertical z levels, which is nearly sufficient to resolve the first baroclinic mode (see, e.g., Stewart et al., 2017). The Gent-McWilliams (GM) parameterization (Gent & McWilliams, 1990) for eddy transport is used, with maximum diffusivity of $1,500 \text{ m}^2/\text{s}$. The GM diffusivity is smoothly reduced with increasing resolution and in vertical direction, as described by Wang, Danilov, et al. (2014). The isoneutral diffusivity takes the same values. Note that we present the results obtained from the recent version of AWI-CM. It uses the KPP mixing scheme instead of the mixing scheme by Pacanowski and Philander (1981) in Sidorenko et al. (2015), which results in a stronger AMOC. The KPP vertical mixing scheme (Large et al., 1994) is used with the background diffusivities of $\sim 1. \text{e} - 5 \text{ m}^2/\text{s}$ (as a function of depth), which is set to smaller values ($\sim 1. \text{e} - 6 \text{ m}^2/\text{s}$) in the Arctic Ocean. The sea ice component of the model (Finite-Element Sea Ice Model) is described in Danilov et al. (2015). It is a subroutine of FESOM, with the thermodynamic part split between FESOM and ECHAM.

The atmospheric component of AWI-CM is the ECHAM6 model, developed at the Max-Planck-Institute for Meteorology (MPI) in Hamburg (Stevens et al., 2013). ECHAM6 is a spectral atmospheric model and can be used in several configurations that differ in the spectral truncation, vertical discretization, associated resolution dependent time step, and in parameters. In the present study, we use the T63 and T127 configurations, which correspond to horizontal resolutions of about 1.9° and 0.9° , respectively. Both configurations have 95 vertical levels and resolve the atmosphere up to 0.01 hPa (about 80 km). The coupling frequency between ocean and atmosphere is 1 hr in all the simulations.

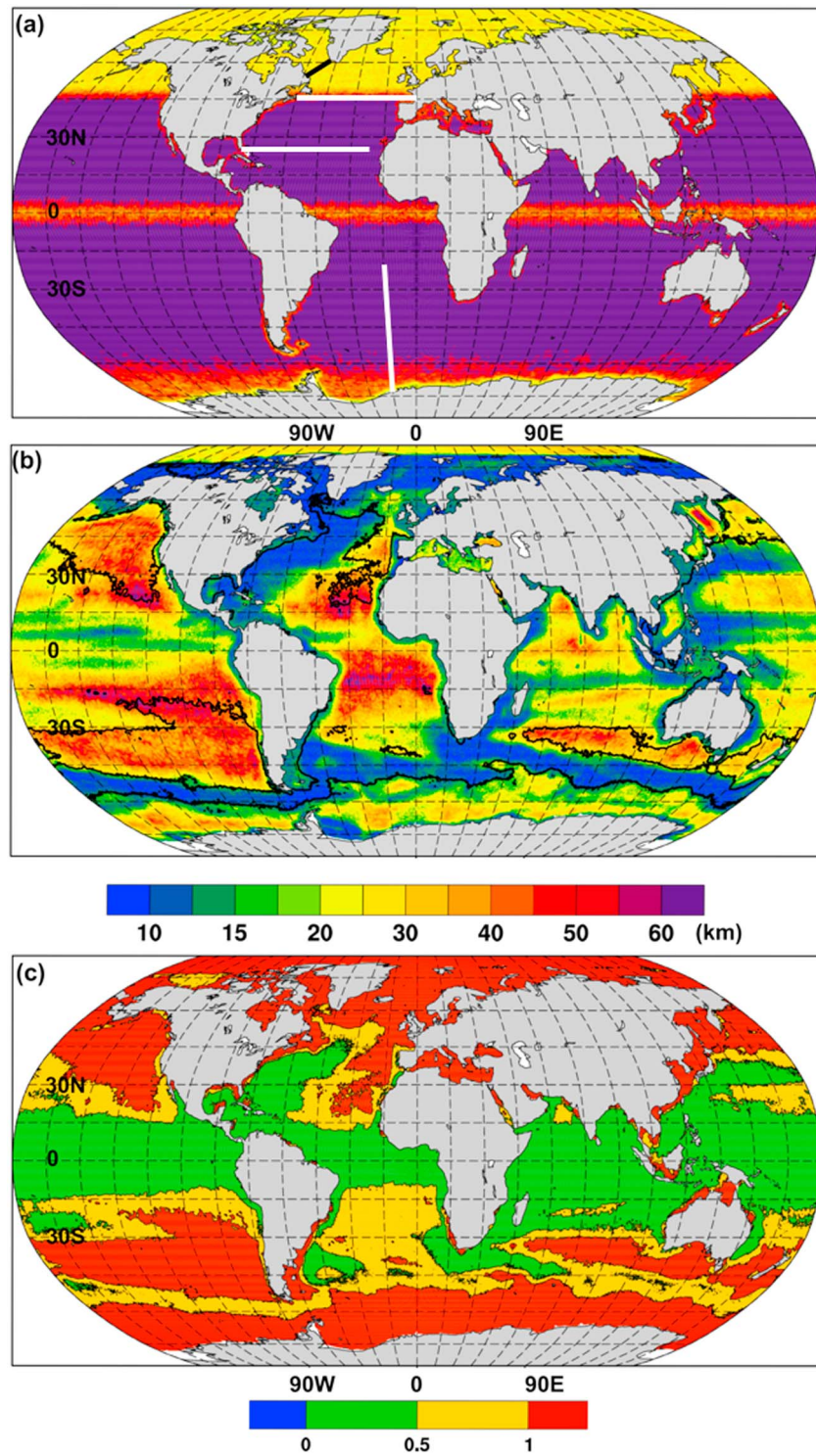


Figure 1. Ocean horizontal resolution in (a) low-resolution (LR) and (b) high-resolution (HR) FESOM setups. The white meridional line on the LR map in the Southern Ocean shows the position of the meridional transect along 15°W. The white line in the North Atlantic shows the position of the zonal transect along 20°N. The contour line in the bottom plot depicts the boundary where resolution coincides with the internal Rossby radius. (c) HR divided by the Rossby radius (Sein et al., 2016).

In order to investigate the impacts of ocean and atmospheric model resolution separately, we use four different coupled setups combining relatively LR and HR configurations of FESOM and ECHAM6: LR/T63, LR/T127, HR/T63, and HR/T127. AWI-CM simulations were carried out close to the HighResMIP protocol (Haarsma et al., 2016): first, the uncoupled ocean was spun-up for 10 years starting from mean 1950–1954 conditions of the EN4 ocean reanalysis (Good et al., 2013) and driven by the CORE II forcing (Large & Yeager, 2009) for the year 1950. Then, the coupled AWI-CM was spun-up for 50 years with atmospheric greenhouse gas concentrations fixed at 1950 levels. After the spin-up, the model was run with historical CMIP5 forcing for the period 1950–2005. At the time of writing this manuscript, the historical CMIP6 forcing had not yet been available.

3. Results

The mean AMOC for the period 1980–2005 simulated with four configurations of AWI-CM is shown in Figures 2a–2d. All runs reproduce the canonical pattern of AMOC reported in literature, depicting a basin-wide middepth cell with a maximum at $\sim 40^\circ\text{N}$ varying from 12 to 20 Sv between realizations. Two bottom rows in Figure 2 show the differences due to the change in the resolution of the ocean (Figures 2e and 2g) and the atmosphere (Figures 2f and 2h). Although there is some difference in details, the left and the right difference patterns are remarkably consistent. This implies that the modification in AMOC caused by the change in ocean resolution is largely independent from the resolution of the atmosphere, and vice versa.

There are several distinct features in the AMOC difference patterns caused by the change in ocean resolution (LR–HR). In general, the HR simulations demonstrate more details, which can be related to sharper currents and difference in representing topography. They have a stronger bottom circulation cell, especially between the equator and 40°N , and stronger AMOC around 2,000-m depths and 20°N , but demonstrate a weaker circulation at latitudes that correspond to the Labrador and Nordic Seas. Concurrently, the most striking difference between simulations using the same ocean but different atmospheres is the strength of the upper cell. It differs substantially, and for both LR and HR ocean resolutions the upper cell of the AMOC is stronger when the coarser (T63) atmospheric resolution is used.

Climate models in general tend to underestimate the AMOC (Wang, Zhang, et al., 2014), and the previous AWI-CM version was no exception in this regard, simulating a maximum AMOC of ~ 12 Sv in the standard configuration (Sidorenko et al., 2015). Estimates from the Rapid Climate Change–Meridional Overturning Circulation and Heatflux Array are in the range of 18.7 ± 2.1 Sv (Kanzow et al., 2010). Further decrease of the AMOC strength with increase of atmospheric resolution may move a coupled model solution in the direction when it becomes more susceptible to change under varying forcing conditions. Along these lines, Sidorenko et al. (2015) discuss the possible collapse of the deep convection in the Labrador Sea caused by an increased freshwater export through Fram Strait. Understanding why and how the AMOC varies with resolution enhances the reliability of our conclusions derived from inspecting numerical experiments.

Several possible reasons for long-term changes in the AMOC strength are discussed in literature: changes in the representation of the ocean topography (as suggested by Winton et al., 2014, and Hewitt et al., 2016), modification of the deep water convection in the NA, and changes in the wind stress that directly drive surface ocean currents. The effects from these changes especially in wind stress can be nonlocal and link changes occurring in the other oceans. The comparison above suggests that the AMOC reacts differently to the resolution in the ocean and atmosphere. Furthermore, the responses combine multiple processes. Indeed, the complicated pattern of AMOC change between LR and HR oceans in the difference panels of Figure 2 can hardly be attributed to a single factor, so that separate explanations for the local extrema seen in these patterns are required. Before discussing response to atmosphere resolution we begin with a qualitative description of the AMOC response to the changes in ocean resolution.

3.1. Ocean Resolution

Three main details are seen in the two bottom left panels of Figure 2: (i) the strengthening of the deep cell in HR (3,000- to 5,000-m range), (ii) the deeper southward flow of the upper cell in HR at depths about 2,000 m (from about 0° to 30°N), and (iii) the stronger upper cell in LR at the latitudes of the Labrador Sea and Grand Banks (200- to 2,000-m range from about 35°N to 60°N).

The strengthening of the deep cell for the HR ocean is already apparent in the full AMOC patterns. We relate this to the change in the frontal structure and the slope of outcropping isopycnal layers in the Southern

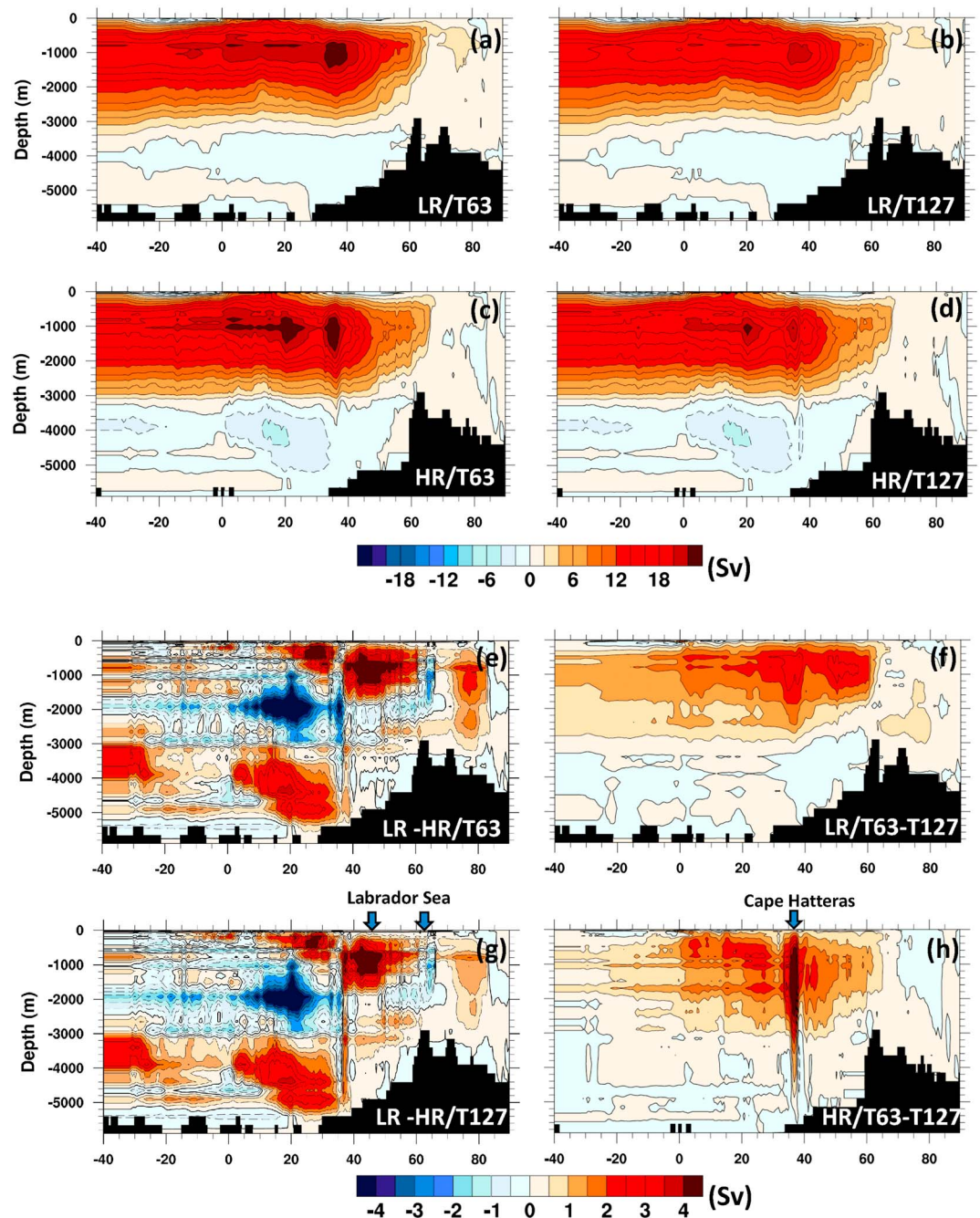


Figure 2. (a–d) Mean (1980–2005) Atlantic meridional overturning circulation for different setups and the difference between setups with (f and h) the same atmosphere but different ocean and (e and g) the same ocean but different atmospheric resolution.

Ocean. The HR ocean is locally eddy resolving in the Agulhas retroflection and Brazil-Malvinas Confluence regions, and thus, simulated eddy variability compares with the observed variability, albeit staying on the lower side (see Sein et al., 2016). We hypothesize that the eddy-induced transport acts to maintain shallower isopycnal slopes, which stay closer to climatology, exemplifying the effect of eddy compensation of the tendency to steepening. Figure 3 presents sections of potential temperature taken along the 15°W transect (position is shown on Figure 1). Clearly, the slope of isothermal surfaces at the front around 40°S separating warm waters from the Antarctic Bottom Water is much steeper in the LR ocean, indicating that

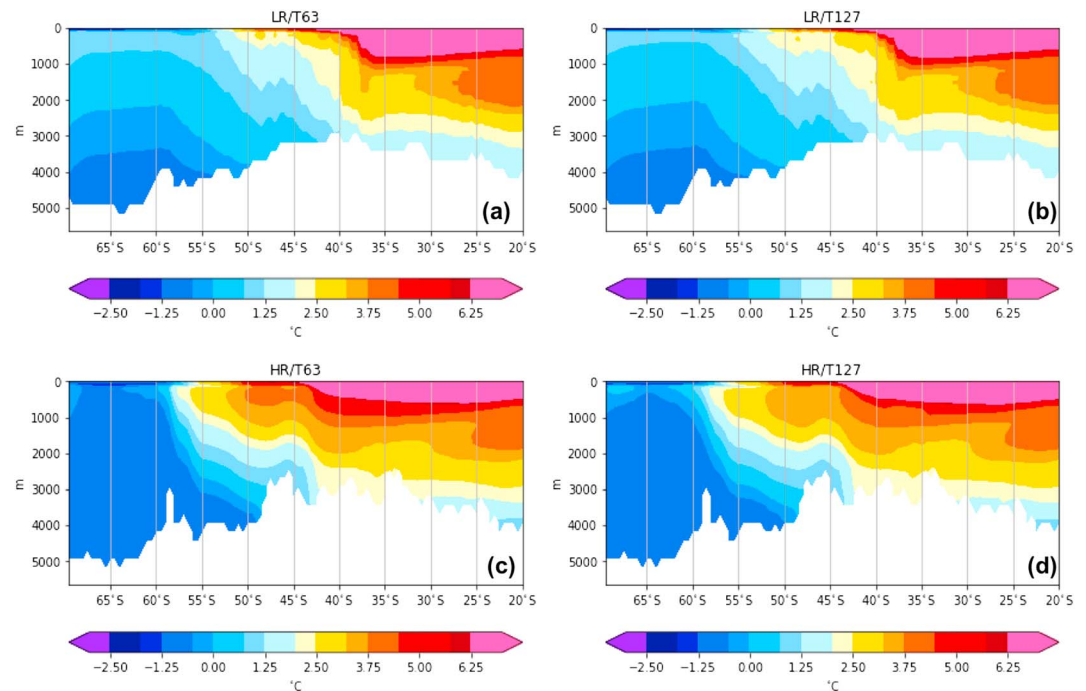


Figure 3. Section of the mean (1980–2005) potential temperature along 15°W, spanning from 70°S to 20°S. Position of the section is shown on Figure 1.

the GM parameterization in the LR simulations is much less effective in counteracting wind-induced steepening. The similar effect was shown by Griffies et al. (2015) where authors presented the 730-m temperature biases for different ocean model resolutions. They demonstrated that the warm 730-m ocean bias in the South Atlantic can be substantially reduced in case of eddy-resolving ocean. Note that the HR runs maintain much sharper gradients between the Antarctic Bottom Water and the rest of the ocean. We suppose that this is the reason why the bottom cell is virtually absent in LR, independent of the atmospheric resolution.

The deeper southward flow in HR simulations (the blue spot in the difference patterns in Figure 2 around 2,000-m depth) can be partly related to the strengthening of the deep cell mentioned above. However, a more plausible reason is the representation of the bottom topography at the latitudes of the Caribbean basin in the LR mesh, which is too coarse in this area, so that part of the Deep Western Boundary Current (DWBC) flows along the submerged topographic features. Furthermore, the higher resolution in HR affects the representation of the DWBC: it is sharper (but weaker) in HR close to the slope and its core is located deeper than in LR (see Figure 4, showing the meridional velocity through the section along 20°N).

In order to check if large AMOC differences are actually translating into transport differences in the depth range associated with the southward transport of deep waters we have calculated total mean (1980–2005) volume transports through portion of the section along 20°N that is bounded by 75°W and 16°W longitude and 1,000- to 3,000-m depth, the depth range where the negative AMOC differences are mostly located (Figure 2). The difference in the subsection volume transport between LR/T63 (−20.75 Sv) and HR/T63 (−18.26 Sv) is about −2.5 Sv. This is smaller than the difference between AMOC values for the models (Figure 2e), which is well over 4 Sv almost through the whole 1,000- to 3,000-m depth range at 20°N. The difference in volume transport between LR/T127 (−18.97 Sv) and HR/T127 (−19.67 Sv) is smaller and has a different sign +0.7 Sv, while the structure and the strength of the AMOC difference are very similar to the T63 results (Figure 2g).

From the comparison of the 1,000- to 3,000-m volume transport differences and the meridional velocity transect along 20°N (Figure 4) it seems plausible that negative AMOC differences between models with LR and HR oceans centered over 20°N and 2,000-m depth are related to the differences in model topography.

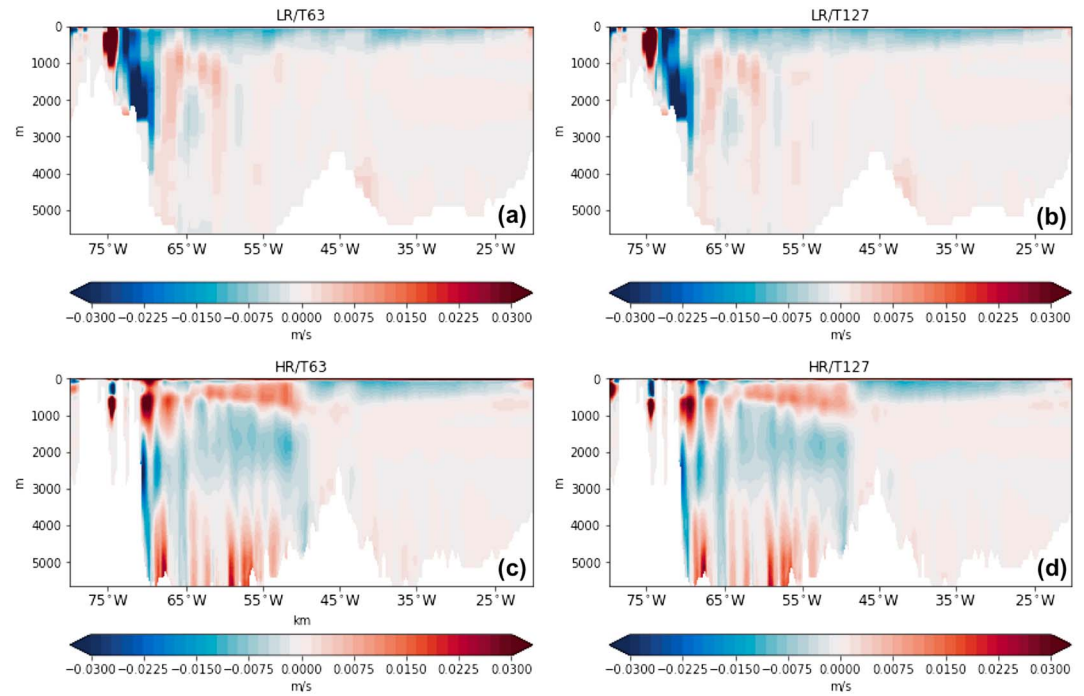


Figure 4. Section of the mean (1980–2005) meridional velocity along 20°N, spanning from 80°W to 20°W. The position of the section is shown in Figure 1.

The stronger upper cell in LR at the latitudes of the Labrador Sea and Grand Banks as compared to HR can be partly related to the strength of the deep water formation. One of the main indicators of the strength of deep water formation in the NA is the mixed layer depth (MLD). Another indicator is the surface water mass transformation (WMT; e.g., Myers & Donnelly, 2008; Paquin et al., 2016; Speer & Tziperman, 1992). It is defined as the cross-isopycnal volume flux due to buoyancy forcing in the surface layer, computed by integrating the buoyancy flux over the surface area A between two isopycnals σ and $\sigma + \Delta\sigma$:

$$F(\sigma) = \frac{1}{T} \int_0^T \left[\frac{1}{\Delta\sigma} \int_{A(\sigma)}^{A(\sigma+\Delta\sigma)} \left(\frac{\alpha}{c_w} Q_H - \rho\beta S Q_F \right) dA \right] dt,$$

where Q_H and Q_F are heat and freshwater fluxes, respectively. The α and β are the thermal and haline expansion/contraction coefficients, respectively. The ρ , c_w , S , and T denote the surface density, the specific heat capacity of water, the surface salinity, and the integration time, respectively.

Figure 5 shows the mean winter MLD for 1980–2005 in all simulations. Differences in the Labrador Sea MLD are much larger between the configurations with different ocean resolutions than between configurations with the same ocean but different atmospheres. The same holds for the winter mean Labrador Sea WMT (Figure 6a), which is negative, indicating a removal of buoyancy, and ranges between surface densities of ~ 27.1 and 28 kg/m^3 . Low (high) ocean resolution leads to higher (lower) WMT; in particular, a much denser (lighter) volume of waters is produced. Although the overturning circulation is largely related to the deep water convection in the Labrador Sea, convection does not imply net sinking, and the relationship might be indirect (e.g., Marotzke & Scott, 1999). Nevertheless, the denser WMT associated with deeper MLD in the LR experiments leads to a stronger southward boundary current transport of the subpolar gyre. In particular, southward volume transport through section AR7W (connecting the southern tip of Greenland with the Labrador coast, black line in Figure 1) amounts to 62, 63, 53, and 49 Sv in experiments LR/T63, LR/T127, HR/T63, and HR/T127, respectively. Note that observations indicate a high variability of the southward boundary current transport through AR7W, ranging between 22 and 57 Sv for the years 1995–2008 (Hall et al., 2013). The higher transport in the LR runs is consistent with a strengthening of the upper AMOC cell at the locations south of where MLD is deeper in experiments with fixed atmospheric resolution.

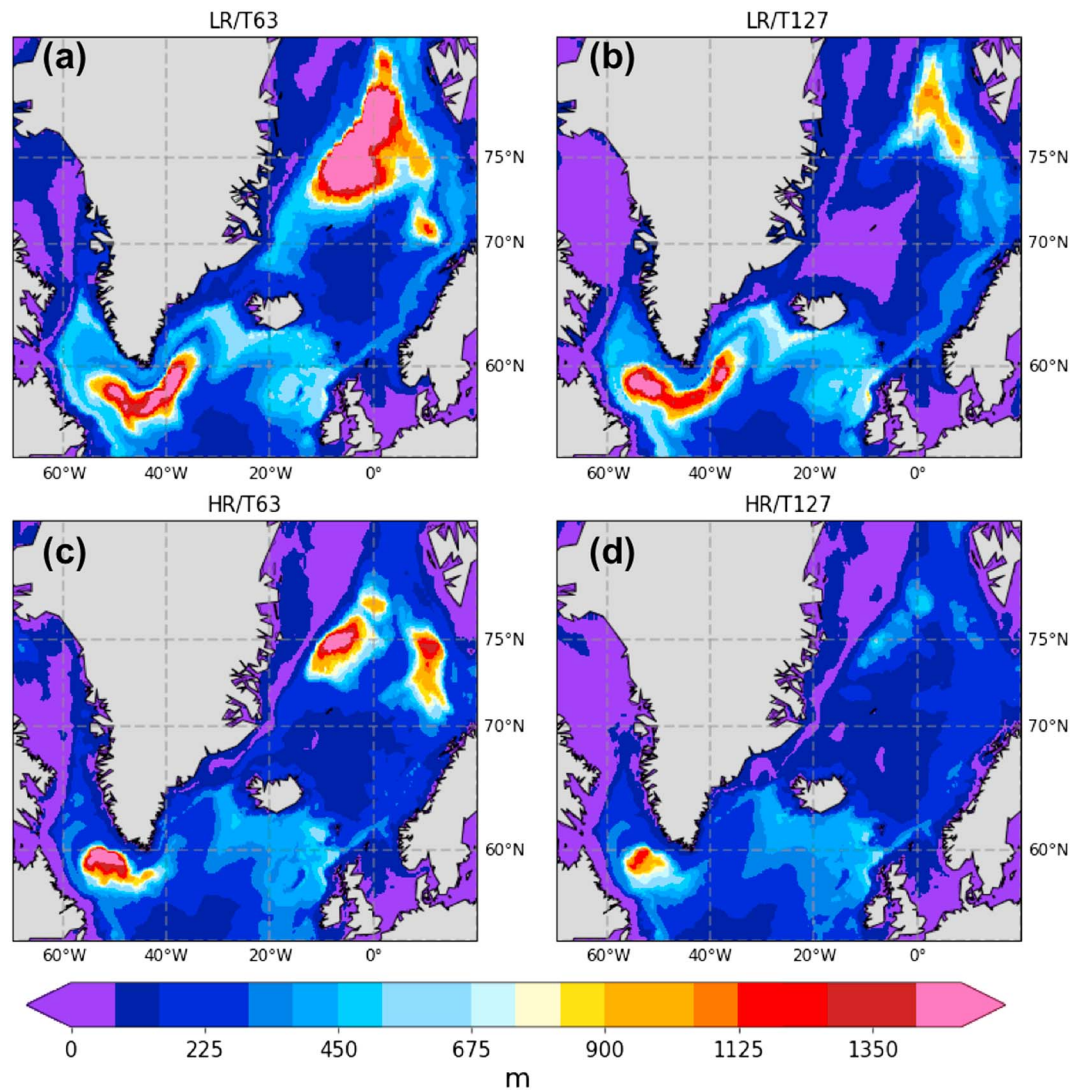


Figure 5. Mean winter mixed layer depth for 1980–2005.

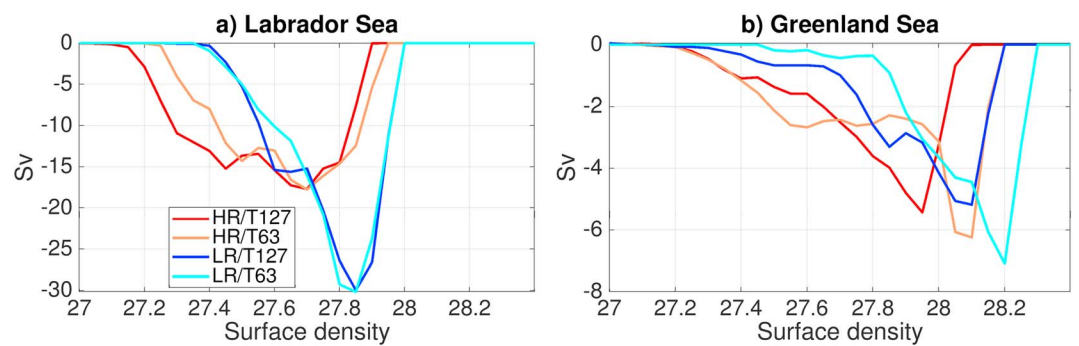


Figure 6. Surface-forced water mass transformation per density class ($\Delta\sigma = 0.1 \text{ kg/m}^3$) averaged over the (a) Labrador Sea ($65\text{--}46^\circ\text{W}$, $50\text{--}65^\circ\text{N}$, water depth $> 1,500 \text{ m}$) and (b) Greenland Sea ($15^\circ\text{W}\text{--}15^\circ\text{E}$, $72\text{--}80^\circ\text{N}$, water depth $> 1,500 \text{ m}$) for the time period March 1980–2005 in experiments HR/T127 (red), HR/T63 (orange), LR/T127 (blue), and LR/T63 (cyan). Negative values indicate a removal of buoyancy.

In the GIN seas, the MLD is sensitive to both the ocean and the atmosphere, being deeper in LR runs and for lower resolution in the atmosphere (Figure 5). This is also reflected in the WMT, with denser volume of waters produced both with lower resolution in the ocean and in the atmosphere (Figure 6b). Consistent with the MLD and WMT differences, the LR-HR difference pattern shows a small cell at the latitudes of the GIN seas. However, the differences in MLD and WMT between the experiments are not reflected in overflow water (OW) volume transport across the Denmark Strait, the main connection to the NA. OW volume transport (defined by densities higher than 27.8 kg/m^3) amounts to 3.5, 2.9, 3.7, and 3.2 Sv in experiments LR/T63, LR/T127, HR/T63, and HR/T127, respectively (note that all transports are in the range of observations, 3.2 ± 0.5 Sv; Jochumsen et al., 2017). Hence, transport is higher with higher ocean resolution and lower atmospheric resolution. In the case of finer ocean resolution, the better resolved bathymetry of the Denmark Strait sill allows for higher throughflow, whereas the lower WMT upstream does not play a role. In the case of lower atmospheric resolution, the higher OW transport can be related to the difference in mean winds. We thus conclude that in our experiments, convection in the GIN seas does not have an impact on the NA.

The stronger upper AMOC cell in LR models has its maximum at about 45°N , which is well to the south of the Labrador Sea. This indicates that it is only partly related to water formation processes discussed above. Another factor explaining it is the difference in the configuration of the ocean circulation at this latitude. Figure 7a shows the position of the 12°C isotherm at 400 m that is often used as an indication of the Gulf Stream position in the western part of the NA. In the eastern part of the NA it can serve as an indicator of the pathway of the NA current. The Gulf Stream pathways start to deviate significantly between models of different ocean resolution starting at 50°W and later the NA current crosses the 45°N latitude already more than 10° apart. A meridional velocity transect along 45°N (Figures 7c–7f) shows that the core of the northward flowing NA current in the eastern part of the Atlantic in HR runs is located at about $30\text{--}32^\circ\text{W}$, over the well-resolved Mid-Atlantic Ridge and confined to the upper 500 m. In LR runs the NA current crosses 45°N at about 18°W and its core spans from the surface to about 1,000 m. The mismatch between vertical extent of the NA current due to difference in the horizontal ocean circulation is therefore partly responsible for the stronger upper AMOC cell.

To conclude, it is important to note that AMOC differences in the upper 3,000 m between ocean models with different resolutions are local and do not propagate further south, hence do not result in the changes in the total water transport between the hemispheres. As shown above, most of these differences are related to horizontal and vertical redistribution of flows due to topography or model dynamics and have no or little effect on net transport. The AMOC differences below 3,000 m are partly related to the Southern Ocean dynamics, in particular, to resolving (HR)/parameterizing (LR) of eddies. However, even here, there are local contributions related to bottom topography, leading to local recirculation such as the one seen around 20°N .

3.2. Atmospheric Resolution

The change in atmospheric resolution affects the middepth cell of the AMOC. The likely reason for the observed AMOC decrease with increased atmospheric resolution is the change in the amount of mechanical energy that is transferred from the atmosphere to the ocean. The higher resolution atmospheric model is expected to better reproduce details of medium-scale atmospheric circulation including better representation of cyclones. Figure 8 shows the standard deviation of band-pass filtered (2.5–6 days) 500-hPa geopotential height, which is often used as a diagnostic for storm activity (Blackmon, 1976). In general, changes between runs with the same ocean but different atmosphere show that storm activity in T63 runs is noticeably weaker over the NA compared to T127 runs (Figure 8, right column). Details of the spatial distribution of storm track differences depend on ocean resolution. Indeed, difference in ocean resolutions affects the spatial distribution of oceanic SST fronts and hence influences position of storm tracks.

The regime with more cyclones is more *chaotic*, and as a result the mean winds become weaker in the HR simulations. Figure 9 shows that wind speed over the typical path of the midlatitude cyclones over the central NA is larger in T63 simulations, especially close to the European coast. This is the region of the NA current, which in large determines the strength of the AMOC. Directly over the Gulf Stream area the 10-m wind differences do not behave consistently between HR and LR runs, with weaker wind speeds in LR/T63 compared to LR/T127 and larger wind speeds in HR/T63 compared to HR/T127. It is interesting to note that spatial patterns of 10-m wind speed distribution over the midlatitudes of the NA (North Atlantic Current) are much more similar in runs with the same ocean than in runs with the same atmosphere. Note that in order to simplify the

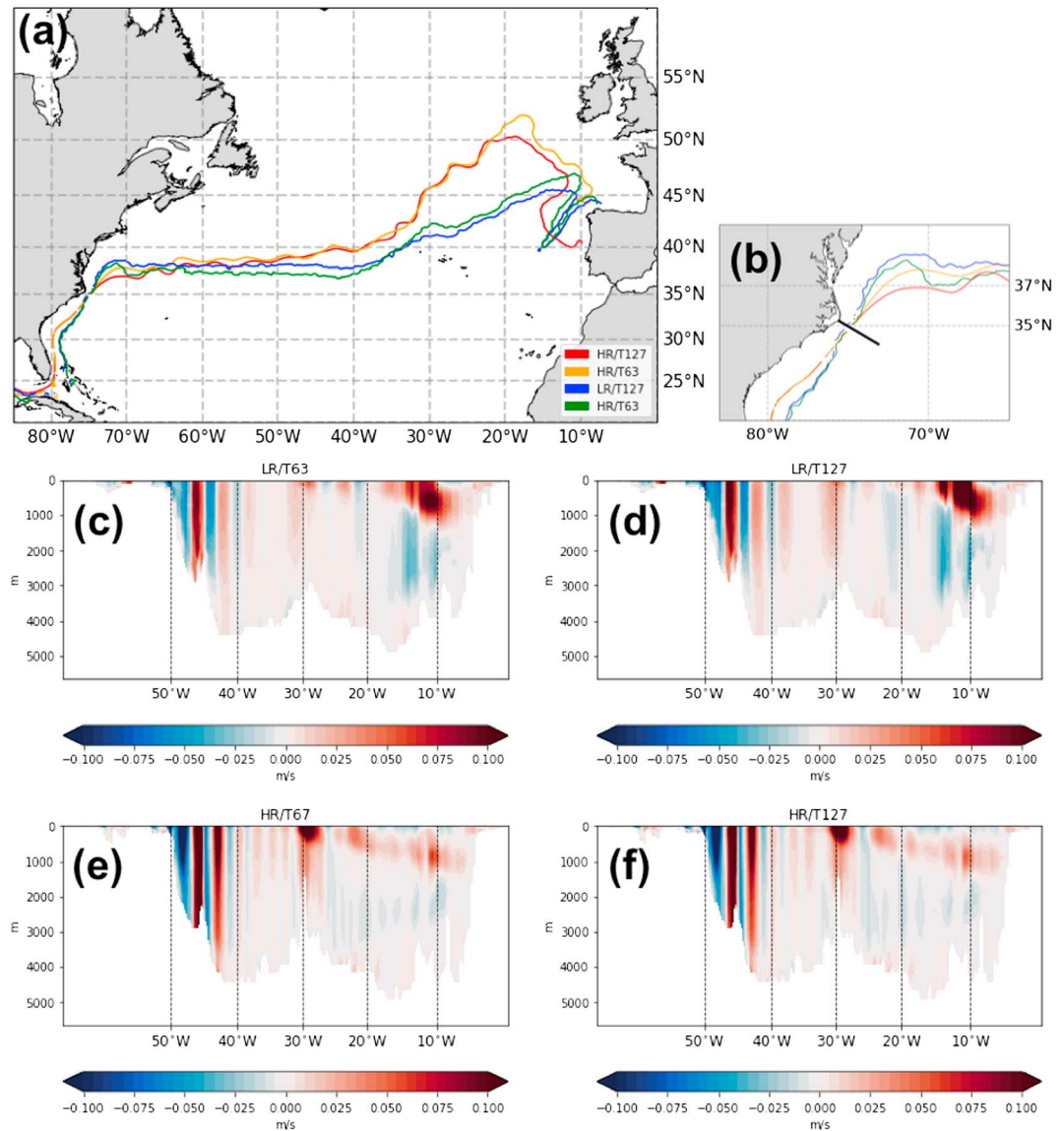


Figure 7. (a and b) Positions of the mean (1980–2005) 12 °C isotherm at 400-m depth in the North Atlantic. The right panel zooms to the Gulf Stream separation region and shows position of the transect over which the transports were calculated. (c–f) Sections of the mean (1980–2005) meridional velocity along 45°N, spanning from 65°W to 0° for different simulations. The position of the section is shown in Figure 1.

analysis presented in the manuscript, the ocean surface currents were not used for calculating the wind stress in the model simulations. Concurrently, Renault et al. (2016) demonstrates that considering the ocean velocities will modify the energy transfer from the atmosphere to the ocean to damp the oceanic eddies. The role of the ocean surface currents in the wind stress computation under different oceanic resolutions is left for future studies.

While the AMOC difference in LR/T63-LR/T127 is relatively smooth, a strong narrow *band* (more than 4 Sv) is observed at approximately 37°N for HR/T63-HR/T127 (Figure 2). Happening slightly north of Cape Hatteras (CH), such change indicates the differences in Gulf Stream separation between HR/T63 and HR/T127 setups, which are clearly illustrated in Figure 10. The North-West transport through the section perpendicular to the main Gulf Stream flow (shown on Figure 7b) amounts to 59.1 and 58.3 Sv for HR/T127 and HR/T63, and the transport difference between experiments is too small to explain the sudden change in AMOC. Figure 7b shows a map of Gulf Stream positions in different experiments (defined as 12 °C isotherm at 400 m),

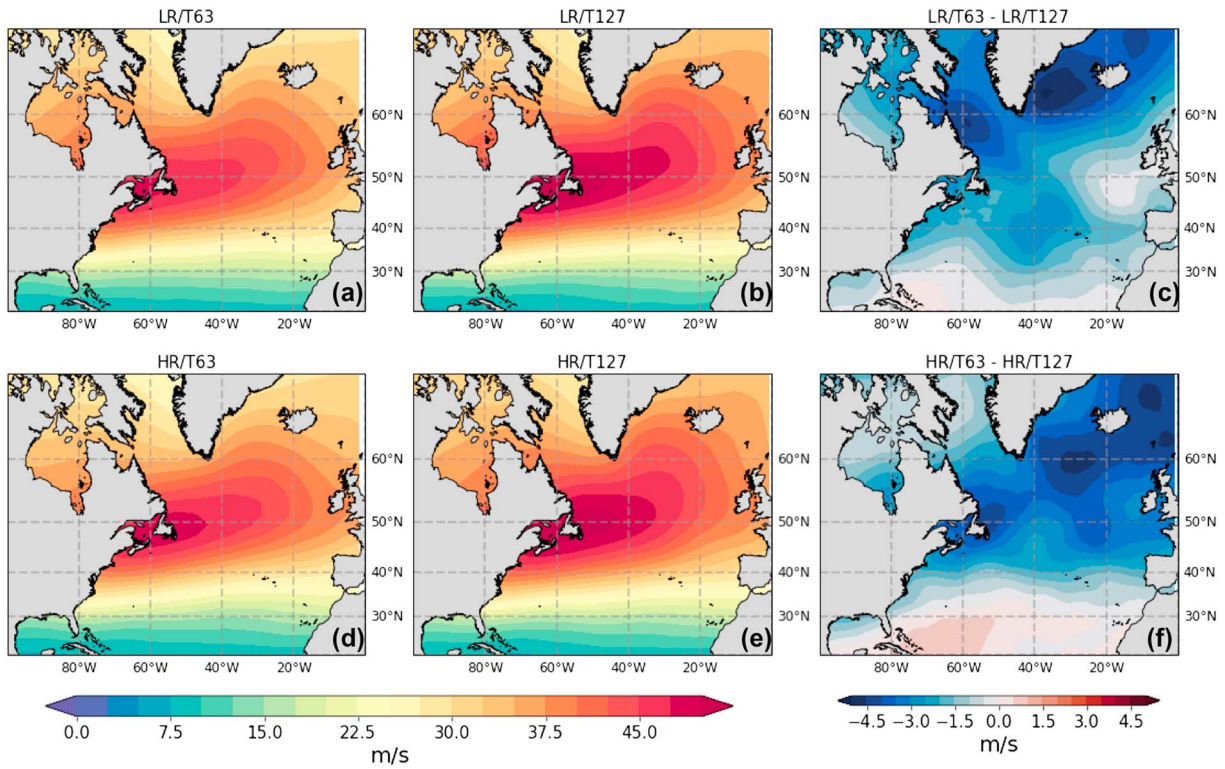


Figure 8. Standard deviation of band-pass filtered (2.5–6 days) 500-hPa geopotential height and its difference between T63 and T127 simulations for the (a–c) low-resolution (LR) and (d–f) high-resolution (HR) ocean.

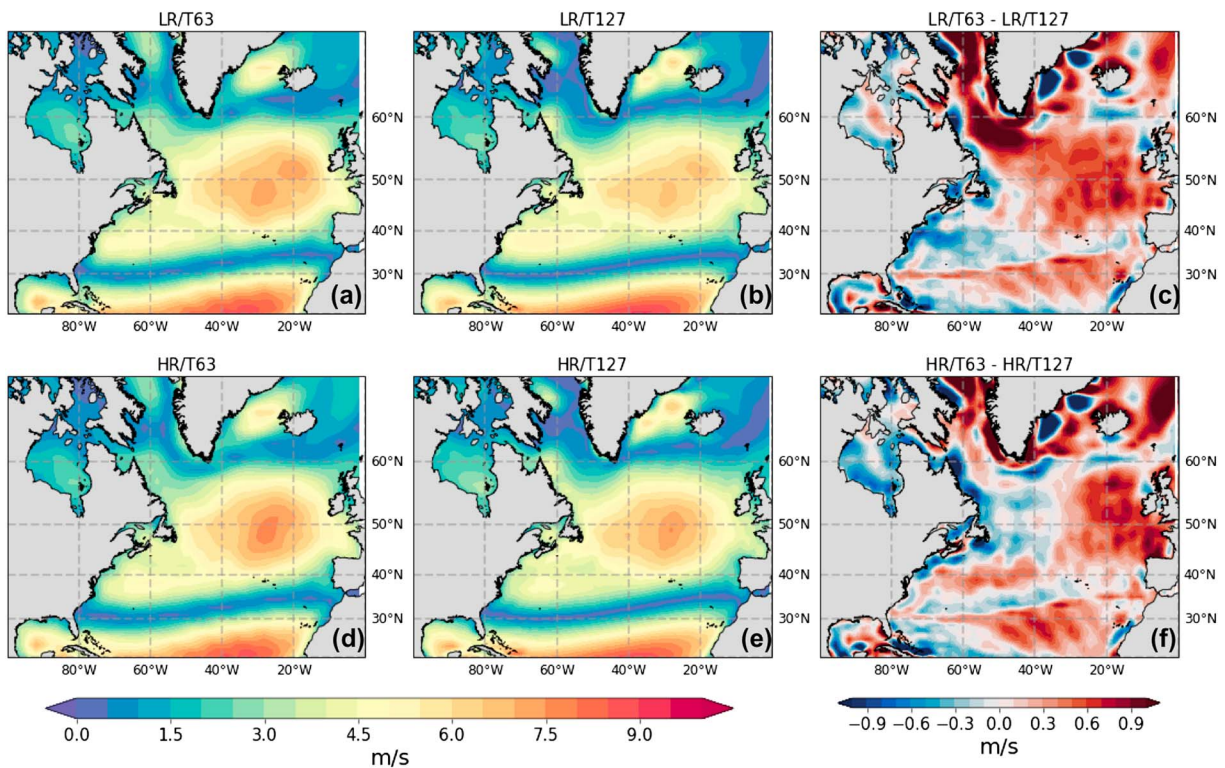


Figure 9. The 10-m wind speed and its difference between T63 and T127 simulations for the (a–c) low-resolution (LR) and (d–f) high-resolution (HR) ocean.

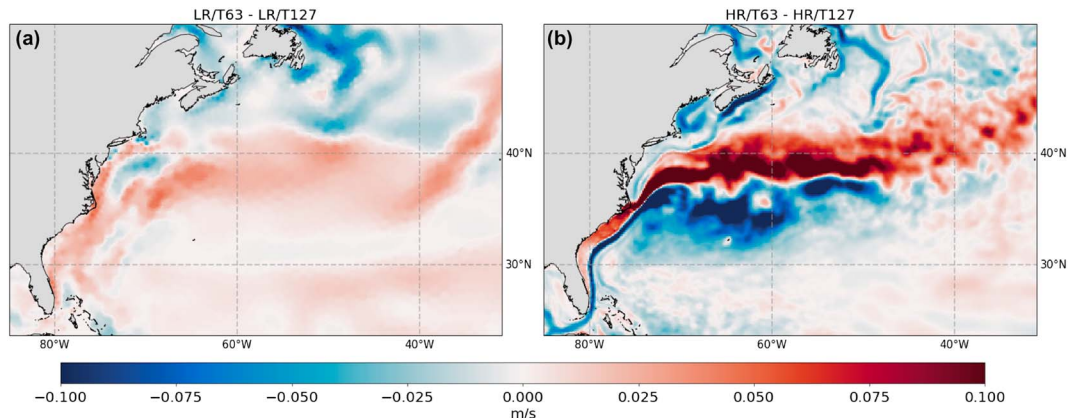


Figure 10. Ocean 50-m velocity differences. (a) LR/T63-LR/T127; (b) HR/T63-HR/T127.

zoomed to the region of the Gulf Stream Separation. It is clear that in HR/T63, the Gulf Stream crosses the 37°N much earlier, which causes the strong local increase of AMOC difference between HR experiments.

Interestingly, this change does not happen if the LR ocean configuration is used. The most plausible explanation is that in the LR setup the ocean resolution is coarse in the vicinity of the Gulf Stream separation at CH and, consequently, the change in mean winds in the atmospheric component of AWI-CM cannot modify the separation. LR has a higher biharmonic viscosity compared to HR (it is scaled with the cube of mesh element size), and due to the no-slip boundary condition of FESOM, viscous terms may dominate the flow in the vicinity of separation. The other factor is a smoother representation of bottom topography on the coarse mesh, which may also affect the response to winds. Additionally, there are nonlocal effects, for example, related to the representation of the continuation of the Labrador Current, which pushes the Gulf Stream away from the CH, which is nearly absent in LR independent of the atmospheric resolution.

In order to illustrate the impact of the mean winds onto the AMOC strength we conducted two additional experiments using the sea ice–ocean model FESOM forced by a prescribed atmosphere. In the reference simulation we force FESOM with the original CORE-II (Large & Yeager, 2009) forcing for the years 1948–2007. In the sensitivity run the 10-m winds were reduced by 20% in the NA. The barotropic and baroclinic responses to wind speed reduction are illustrated in Figure 11 by showing the corresponding changes in SSH (left panel) and AMOC (right panel), respectively. In the SSH, the major change is seen in the NA and is manifested by decrease in the strengths of subtropical and subpolar gyres by 10 and 20 cm, respectively. Simultaneously, the strength of the Beaufort Gyre in the Arctic Ocean has dropped by 5 cm and the accompanied increase of SSH by ~5 cm is found at the adjacent shelves.

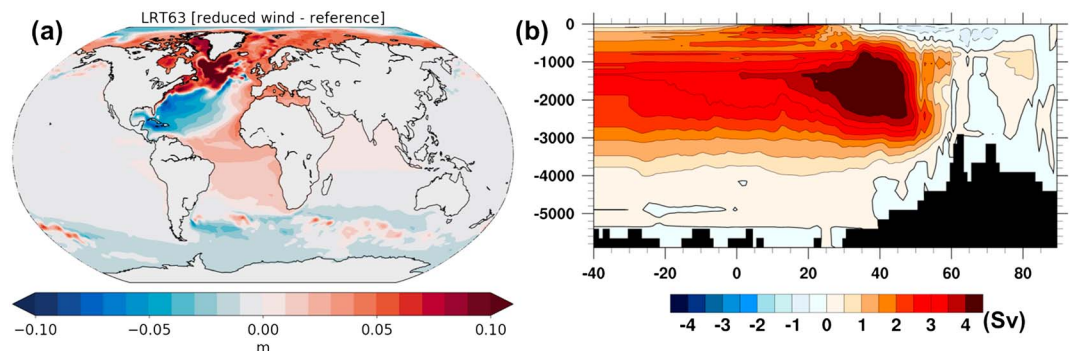


Figure 11. Difference between ocean-only experiments using prescribed atmospheric CORE-II forcing. Original CORE-II forcing was used for the reference simulation. In the sensitivity run the 10-m winds were reduced by 20% in the North Atlantic. (a) The difference in SSH between sensitivity and reference runs averaged over years 2000–2007. Note that sea surface height in the saturated area in Subpolar Gyre reaches 20 cm. (b) The corresponding response in AMOC (reference minus sensitivity shown).

The reduction in wind speeds weakens the gradient between the subtropical and subpolar gyres and consequently the strength of the NA current. This in turn has a tremendous impact on the strength of the simulated AMOC as is shown in Figure 11b. The change in the AMOC is exhibited by a basin-wide decrease of the mid-depth cell reaching a maximum of 5 Sv at about 40°N. The sensitivity experiments confirm that the decrease in the mean wind speeds between T63 and T127 configurations can serve as a plausible explanation for the AMOC reduction.

4. Conclusions

In this paper, we compare the performance of four coupled atmosphere-ocean setups at various different resolutions (HR atmosphere and ocean, LR atmosphere and ocean, HR atmosphere and LR ocean, and LR atmosphere and HR ocean). The resolutions for the atmosphere explored here range from T63 to T127 (nominally 1.9° and 0.9°). The LR ocean mesh is based on a 1° mesh with resolution increased to 25 km north of 50°N, whereas the HR ocean mesh is locally eddy-resolving with the horizontal resolution varying according to the observed SSH. By looking into all possible combinations of high and LR atmosphere and ocean components, we were able to systematically explore the effect of resolution on the simulated climate, separating effects coming from the atmospheric model from the effects introduced by the ocean model. Our focus was on the AMOC, the behavior of which is commonly considered to be of critical importance for describing climate as well as climate change.

The main conclusion that follows from our results is that changes in resolutions of the ocean and the atmosphere affect the AMOC in different and largely independent ways (at least for the range of resolutions studied here and at least in this model). The change in the ocean resolution affects the AMOC in a relatively complicated way, and we were able to propose some plausible explanations for such a behavior. Except for the MLD response, which was probably difficult to anticipate, other effects related to eddy transport and mixing in the Southern Ocean and the pathways of the DWBC and the North Atlantic Current could probably have been expected. The interplay of different processes might be one of the factors additional to the structural differences in the models why there is no consensus in the literature yet on the AMOC response to enhanced resolution in ocean models (Hewitt et al., 2017).

The higher atmospheric resolution leads to weaker AMOC in response to weaker mean winds associated with higher cyclone activity. Interestingly, in uncoupled simulations the ocean model response to the higher-resolution atmospheric forcing turns out to be the opposite (e.g., Jung et al., 2014). This difference is likely related to the fact that the wind forcing used to drive stand-alone ocean models is based on reanalysis data. Independent of resolution they rely on assimilated winds, thus keeping their strength on the same level independent of resolution.

Previous studies (e.g., Hewitt et al., 2016; Storkey et al., 2018) point out that increasing ocean resolution leads to increased AMOC. Interestingly, we do not see this in our simulations. As mentioned above, we cannot propose a plausible explanation to the observed MLD behavior in our simulations, which might be related to additional factors such as the sea ice and hydrological cycle. Furthermore, the range of atmospheric resolutions explored by us is still lower than that explored in the Hewitt et al. (2016) setup; it cannot be excluded that the sensitivity to the change in resolution is different, if relatively coarse resolutions are explored (T63 vs T127). Moreover, differences between AWI-CM and GC2 model used by Hewitt et al. (2016) might play a role, which calls for more systematic, coordinated multimodel experiments.

Another interesting finding is that the HR atmosphere further improves the pathway of the Gulf Stream only in the case when the ocean model resolution is already sufficiently high to reproduce its separation correctly. We hypothesize that too high viscosity together with the no-slip boundary condition is the main reason for suppressing the reaction of the LR ocean to the higher-resolved atmosphere.

Note that some of the changes in the AMOC seen in our simulations are confined to the Northern Hemisphere. Weak interhemispheric signal is seen only in the appearance of weak deep cell in the HR ocean and in the reduced upper cell for the higher resolution atmosphere. More research is needed toward understanding the role of local versus interhemispheric changes in shaping the climate signal, which will be addressed in future research.

To conclude, we see that a change in atmospheric versus oceanic resolution leads to systematic changes in the AMOC (and other diagnostics not discussed here). We should point out that our results are based on a single climate model, which raises the question whether our findings are model dependent. In this context, it is worth pointing out that ongoing work in the framework of the HighResMIP project and its European part PRIMAVERA will produce a set of HR and LR coupled simulations that can be used for further investigations in a multimodel context.

Another interesting question is how these changes affect the simulated climate change signal. We believe that the results and sensitivities presented here might be helpful in this context, and we leave the discussion of potential impacts on climate change projections for future studies.

Acknowledgments

We thank Helene Hewitt, anonymous reviewer, and Associated Editor for their very helpful comments. The work was supported by the EC project PRIMAVERA under the grant agreement 641727 (D. Sein, T. Jung, and T. Semmler), by projects S1 (N. Koldunov and T. Jung) and S2 (S. Danilov and P. Scholz) of the Collaborative Research Centre TRR 181 “Energy Transfer in Atmosphere and Ocean” funded by the German Research Foundation, by the Helmholtz Climate Initiative REKLIM (Regional Climate Change; D. Sidorenko and Q. Wang), by the FRontiers in Arctic marine Monitoring program (FRAM, C. Wekerle), the state assignment of FASO Russia (theme 0149-2018-0014 and by ERA-Net projects EXOSYSTEM (grant agreement 01DJ16016), and FRAGERUS (grant agreement 01DJ15029) funded by the Federal Ministry for Education and Research (Germany). The simulations were performed at the German Climate Computing Center (DKRZ). The data are available at https://swiftbrowser.dkrz.de/public/dkrz_035d8f6ff058403bb42f8302e6badfbc/SEIN_AMOC_JAMES2018/.

References

- Blackmon, M. L. (1976). A climatological spectral study of the 500 mb geopotential height of the Northern Hemisphere. *Journal of the Atmospheric Sciences*, 33(8), 1607–1623. [https://doi.org/10.1175/1520-0469\(1976\)033<1607:ACSSOT>2.0.CO;2](https://doi.org/10.1175/1520-0469(1976)033<1607:ACSSOT>2.0.CO;2)
- Bryan, F. O., Tomas, R., Dennis, J. M., Chelton, D. B., Loeb, N. G., & McClean, J. L. (2010). Frontal scale air–sea interaction in high-resolution coupled climate models. *Journal of Climate*, 23(23), 6277–6291. <https://doi.org/10.1175/2010JCLI3665.1>
- Chang, Y. S., Garraffo, Z. D., Peters, H., & Özgökmen, T. M. (2009). Pathways of Nordic overflows from climate model scale and eddy resolving simulations. *Ocean Modelling*, 29(1), 66–84. <https://doi.org/10.1016/j.ocemod.2009.03.003>
- Danabasoglu, G., Yeager, S. G., Kim, W. M., Behrens, E., Bentsen, M., Bi, D., et al. (2016). North Atlantic simulations in Coordinated Ocean-ice Reference Experiments phase II (CORE-II). Part II: Inter-annual to decadal variability. *Ocean Modelling*, 97, 65–90. <https://doi.org/10.1016/j.ocemod.2015.11.007>
- Danilov, S., Wang, Q., Timmermann, R., Iakovlev, N., Sidorenko, D., Kimmritz, M., et al. (2015). Finite-element sea ice model (FESIM), version 2. *Geoscientific Model Development*, 8(6), 1747–1761. <https://doi.org/10.5194/gmd-8-1747-2015>
- Frenger, I., Gruber, N., Knutti, R., & Münnich, M. (2013). Imprint of Southern Ocean eddies on winds, clouds and rainfall. *Nature Geoscience*, 6(8), 608–612. <https://doi.org/10.1038/ngeo1863>
- Gent, P. R., & McWilliams, J. C. (1990). Isopycnal mixing in ocean circulation models. *Journal of Physical Oceanography*, 20(1), 150–155. [https://doi.org/10.1175/1520-0485\(1990\)020<0150:IMOCM>2.0.CO;2](https://doi.org/10.1175/1520-0485(1990)020<0150:IMOCM>2.0.CO;2)
- Good, S. A., Martin, M. J., & Rayner, N. A. (2013). EN4: Quality controlled ocean temperature and salinity profiles and monthly objective analyses with uncertainty estimates. *Journal of Geophysical Research: Oceans*, 118, 6704–6716. <https://doi.org/10.1002/2013JC009067>
- Griffies, S. M., Winton, M., Anderson, W. G., Benson, R., Delworth, T. L., Dufour, C. O., et al. (2015). Impacts on ocean heat from transient mesoscale eddies in a hierarchy of climate models. *Journal of Climate*, 28(3), 952–977. <https://doi.org/10.1175/JCLI-D-14-00353.1>
- Haarsma, R. J., Roberts, M. J., Vidale, P. L., Senior, C. A., Bellucci, A., Bao, Q., et al. (2016). High resolution model intercomparison project (HighResMIP v1.0) for CMIP6. *Geoscientific Model Development*, 9(11), 4185–4208. <https://doi.org/10.5194/gmd-9-4185-2016>
- Hall, M. M., Torres, D. J., & Yashayaev, I. (2013). Absolute velocity along the AR7W section in the Labrador Sea. *Deep Sea Research Part I: Oceanographic Research Papers*, 72, 72–87. <https://doi.org/10.1016/j.jsr.2012.11.005>
- He, J., Winton, M., Vecchi, G., Jia, L., & Rugenstein, M. (2017). Transient climate sensitivity depends on base climate ocean circulation. *Journal of Climate*, 30(4), 1493–1504. <https://doi.org/10.1175/JCLI-D-16-0581.1>
- Hewitt, H. T., Bell, M. J., Chassignet, E. P., Czaja, A., Ferreira, D., Griffies, S. M., et al. (2017). Will high-resolution global ocean models benefit coupled predictions on short-range to climate timescales? *Ocean Modelling*, 120, 120–136. <https://doi.org/10.1016/j.ocemod.2017.11.002>
- Hewitt, H. T., Roberts, M. J., Hyder, P., Graham, T., Rae, J., Belcher, S. E., et al. (2016). The impact of resolving the Rossby radius at mid-latitudes in the ocean: Results from a high-resolution version of the Met Office GC2 coupled model. *Geoscientific Model Development Discussion*, 1–35. <https://doi.org/10.5194/gmd-2016-87>
- Iovino, D., Masina, S., Storto, A., Cipollone, A., & Stepanov, V. N. (2016). A 1/16° eddy simulation of the global NEMO sea-ice–ocean system. *Geoscientific Model Development*, 9(8), 2665–2684. <https://doi.org/10.5194/gmd-9-2665-2016>
- Jochumsen, K., Moritz, M., Nunes, N., Quadfasel, D., Larsen, K. M., Hansen, B., et al. (2017). Revised transport estimates of the Denmark Strait overflow. *Journal of Geophysical Research: Oceans*, 122, 3434–3450. <https://doi.org/10.1002/2017JC012803>
- Jung, T., Gulev, S. K., Rudeva, I., & Soloviev, V. (2006). Sensitivity of extratropical cyclone characteristics to horizontal resolution in the ECMWF model. *Quarterly Journal of the Royal Meteorological Society*, 132(619), 1839–1857. <https://doi.org/10.1256/qj.05.212>
- Jung, T., Miller, M., Palmer, T., Towers, P., Wedi, N., Achuthavarier, D., et al. (2012). High-resolution global climate simulations with the ECMWF model in Project Athena: Experimental design, model climate and seasonal forecast skill. *Journal of Climate*, 25(9), 3155–3172. <https://doi.org/10.1175/JCLI-D-11-00265.1>
- Jung, T., Serrar, S., & Wang, Q. (2014). The oceanic response to mesoscale atmospheric forcing. *Geophysical Research Letters*, 41, 1255–1260. <https://doi.org/10.1002/2013GL059040>
- Kanzow, T., Cunningham, S. A., Johns, W. E., Hirschi, J. J., Marotzke, J., Baringer, M. O., et al. (2010). Seasonal variability of the Atlantic meridional overturning circulation at 26.5°N. *Journal of Climate*, 23(21), 5678–5698. <https://doi.org/10.1175/2010JCLI3389.1>
- Large, W. G., McWilliams, J. C., & Doney, S. C. (1994). Oceanic vertical mixing: A review and a model with a nonlocal boundary layer parameterization. *Reviews of Geophysics*, 32(4), 363–403. <https://doi.org/10.1029/94RG01872>
- Large, W. G., & Yeager, S. G. (2009). The global climatology of an interannually varying air–sea flux data set. *Climate Dynamics*, 33(2–3), 341–364. <https://doi.org/10.1007/s00382-008-0441-3>
- Ma, X., Chang, R. C., Saravanan, R., Montuoro, R., Hsieh, J.-S., Wu, D., et al. (2015). Distant influence of Kuroshio eddies on North Pacific weather patterns? *Scientific Reports*, 5, 17785. <https://doi.org/10.1038/srep17785>
- Ma, X., Jing, Z., Chang, P., Liu, X., Montuoro, R., Small, R. J., et al. (2016). Western boundary currents regulated by interaction between ocean eddies and the atmosphere. *Nature*, 535, 533–537. <https://doi.org/10.1038/nature18640>
- Marotzke, J., & Scott, J. R. (1999). Convective mixing and the thermohaline circulation. *Journal of Physical Oceanography*, 29(11), 2962–2970. [https://doi.org/10.1175/1520-0485\(1999\)029<2962:CMATTC>2.0.CO;2](https://doi.org/10.1175/1520-0485(1999)029<2962:CMATTC>2.0.CO;2)
- Marzocchi, A., Hirschi, J. J. M., Holliday, N. P., Cunningham, S. A., Blaker, A. T., & Coward, A. C. (2015). The North Atlantic subpolar circulation in an eddy-resolving global ocean model. *Journal of Marine Systems*, 142, 126–143. <https://doi.org/10.1016/j.jmarsys.2014.10.007>

- Myers, P. G., & Donnelly, C. (2008). Water mass transformation and formation in the Labrador Sea. *Journal of Climate*, *21*(7), 1622–1638. <https://doi.org/10.1175/2007JCLI1722.1>
- Pacanowski, R. C., & Philander, S. G. H. (1981). Parameterization of vertical mixing in numerical models of tropical oceans. *Journal of Physical Oceanography*, *11*(11), 1443–1451. [https://doi.org/10.1175/1520-0485\(1981\)011<1443:POVMIN>2.0.CO;2](https://doi.org/10.1175/1520-0485(1981)011<1443:POVMIN>2.0.CO;2)
- Paquin, J. P., Lu, Y., Higginson, S., Dupont, F., & Garric, G. (2016). Modelled variations of deep convection in the Irminger Sea during 2003–10. *Journal of Physical Oceanography*, *46*(1), 179–196. <https://doi.org/10.1175/JPO-D-15-0078.1>
- Rackow, T., Goessling, H. F., Jung, T., Sidorenko, D., Semmler, T., Barbi, D., & Handorf, D. (2016). Towards multi-resolution global climate modeling with ECHAM6-FESOM. Part II: climate variability. *Climate Dynamics*, *50*(7–8), 2369–2394. <https://doi.org/10.1007/s00382-016-3192-6>
- Renault, L., Molemaker, M. J., McWilliams, J. C., Schepetkin, A. F., Lemarié, F., Chelton, D., et al. (2016). Modulation of wind work by oceanic current interaction with the atmosphere. *Journal of Physical Oceanography*, *46*(6), 1685–1704. <https://doi.org/10.1175/JPO-D-15-0232.1>
- Roberts, M. J., Hewitt, H. T., Hyder, P., Ferreira, D., Josey, S. A., Mizielinski, M., & Shelly, A. (2016). Impact of ocean resolution on coupled air-sea fluxes and large-scale climate. *Geophysical Research Letters*, *43*, 10,430–10,438. <https://doi.org/10.1002/2016GL070559>
- Sein, D. V., Danilov, S., Biastoch, A., Durgadoo, J. V., Sidorenko, D., Harig, S., & Wang, Q. (2016). Designing variable ocean model resolution based on the observed ocean variability. *Journal of Advances in Modeling Earth Systems*, *8*, 904–916. <https://doi.org/10.1002/2016MS000650>
- Sein, D. V., Koldunov, N. V., Danilov, S., Wang, Q., Sidorenko, D., Fast, I., et al. (2017). Ocean modeling on a mesh with resolution following the local Rossby radius. *Journal of Advances in Modeling Earth Systems*, *9*, 2601–2614. <https://doi.org/10.1002/2017MS001099>
- Sidorenko, D., Rackow, T., Jung, T., Semmler, T., Barbi, D., Danilov, S., et al. (2015). Towards multi-resolution global climate modeling with ECHAM6-FESOM. Part I: model formulation and mean climate. *Climate Dynamics*, *44*(3), 757–780.
- Small, R. J., Bacmeister, J., Bailey, D., Baker, A., Bishop, S., Bryan, F., et al. (2014). A new synoptic scale resolving global climate simulation using the Community Earth System Model. *Journal of Advances in Modeling Earth Systems*, *6*, 1065–1094. <https://doi.org/10.1002/2014MS000363>
- Small, R. J., deSzoeke, S. P., Xie, S. P., O'Neill, L., Seo, H., Song, Q., et al. (2008). Air–sea interaction over ocean fronts and eddies. *Dynamics of Atmospheres and Oceans*, *45*(3–4), 274–319. ISSN 0377-0265. <https://doi.org/10.1016/j.dynatmoce.2008.01.001>
- Smirnov, D., Newman, M., Alexander, M. A., Kwon, Y. O., & Frankignoul, C. (2015). Investigating the local atmospheric response to a realistic shift in the Oyashio sea surface temperature front. *Journal of Climate*, *28*(3), 1126–1147. <https://doi.org/10.1175/JCLI-D-14-00285.1>
- Speer, K., & Tziperman, E. (1992). Rates of water mass formation in the North Atlantic Ocean. *Journal of Physical Oceanography*, *22*(1), 93–104. [https://doi.org/10.1175/1520-0485\(1992\)022<0093:ROWMFI>2.0.CO;2](https://doi.org/10.1175/1520-0485(1992)022<0093:ROWMFI>2.0.CO;2)
- Stevens, B., Giorgetta, M., Esch, M., Mauritsen, T., Crueger, T., Rast, S., et al. (2013). Atmospheric component of the MPI-M Earth System Model: ECHAM6. *Journal of Advances in Modeling Earth Systems*, *5*, 146–172. <https://doi.org/10.1002/jame.20015>
- Stewart, K. D., Hogg, A. M., Griffies, S. M., Heerdegen, A. P., Ward, M. L., Spence, P., & England, M. H. (2017). Vertical resolution of baroclinic modes in global ocean models. *Ocean Modelling*, *113*, 50–65. <https://doi.org/10.1016/j.ocemod.2017.03.012>
- Storkey, D., Blaker, A. T., Mathiot, P., Megann, A., Aksenov, Y., Blockley, E. W., et al. (2018). UK Global Ocean GO6 and GO7: A traceable hierarchy of model resolutions. *Geoscientific Model Development Discussion*. <https://doi.org/10.5194/gmd-2017-263>
- Von Storch, J.-S., Haak, H., Hertwig, E., & Fast, I. (2016). Vertical heat and salt fluxes due to resolved and parameterised meso-scale eddies. *Ocean Modelling*, *108*, 1–19. <https://doi.org/10.1016/j.ocemod.2016.10.001>
- Wang, C., Zhang, L., Lee, S. K., Wu, L., & Mechoso, C. R. (2014). A global perspective on CMIP5 climate model biases. *Nature Climate Change*, *4*(3), 201–205. <https://doi.org/10.1038/nclimate2118>
- Wang, Q., Danilov, S., Sidorenko, D., Timmermann, R., Wekerle, C., Wang, X., et al. (2014). The Finite Element Sea Ice–Ocean Model (FESOM) v.1.4: Formulation of an ocean general circulation model. *Geoscientific Model Development*, *7*, 663–693. <https://doi.org/10.5194/gmd-7-663-2014>
- Wang, Q., Ilicak, M., Gerdes, R., Drange, H., Aksenov, Y., Bailey, D. A., et al. (2016a). An assessment of the Arctic Ocean in a suite of interannual CORE-II simulations. Part I: Sea ice and solid freshwater. *Ocean Modelling*, *99*, 110–132. <https://doi.org/10.1016/j.ocemod.2015.12.008>
- Wang, Q., Ilicak, M., Gerdes, R., Drange, H., Aksenov, Y., Bailey, D. A., et al. (2016b). An assessment of the Arctic Ocean in a suite of interannual CORE-II simulations. Part II: Liquid freshwater. *Ocean Modelling*, *99*, 86–109. <https://doi.org/10.1016/j.ocemod.2015.12.009>
- Wang, Q., Wekerle, C., Danilov, S., Wang, X., & Jung, T. (2018). A 4.5 km resolution Arctic Ocean simulation with the global multi-resolution model FESOM1.4. *Geoscientific Model Development*, *11*, 1229–1255. <https://doi.org/10.5194/gmd-11-1229-2018>
- Winton, M., Anderson, W. G., Delworth, T. L., Griffies, S. M., Hurlin, W. J., & Rosati, A. (2014). Has coarse ocean resolution biased simulations of transient climate sensitivity? *Geophysical Research Letters*, *41*, 8522–8529. <https://doi.org/10.1002/2014GL061523>